Environ. Sci. Technol. 1994, 28, 53–62

Desorption of Halogenated Organics from Model Solids, Sediments, and Soil under Unsaturated Conditions. 1. Isotherms

James Farrell[†] and Martin Reinhard[*]

Department of Civil Engineering, Stanford University, Stanford, California 94305

Desorption isotherms spanning 4–5 orders of magnitude in vapor concentration were measured for chloroform, trichloroethylene, and tetrachloroethylene under unsaturated conditions at 100% relative humidity. The mechanisms affecting isotherm shape were investigated using model solids, aquifer materials, and soil spanning a range in physical properties. Uptake from the vapor phase was examined in terms of four sorption mechanisms: (1) mineral surface adsorption, (2) partitioning into natural organic matter, (3) partitioning into surface-bound water, and (4) adsorption in micropores. Evidence is presented that a heretofore overlooked mechanism—adsorption in micropores—contributes significantly to sorbate uptake and contributes to isotherm nonlinearity on solids with low natural organic matter contents. Micropores are those pores less than several adsorbate diameters in width and are implicated as showing enhanced adsorption as compared to pores of larger dimension. Isotherm shape on solids with low natural organic matter appears to be dominated by intraaggregate microporosity.

Introduction

Adsorption and desorption processes control both the transport and the fate of soil and groundwater pollutants, and much work has been done to understand the processes and parameters which control organic contaminant sorption on soils and sediments (*1–14*). However, the complexities and inherent heterogeneities of natural systems have precluded the elucidation of the mechanisms governing contaminant uptake and release. In order to understand contaminant behavior in the environment and to develop models for estimating sorption beyond the range of measured data, a mechanistic understanding of sorption processes is essential.

The purpose of this work was to examine the mechanisms responsible for sorption under unsaturated conditions and to clarify the factors affecting isotherm shape. Recent work has attributed nonlinear sorption to heterogeneity at the intraparticle scale. Weber et al. (*14*) assert that heterogeneity among the types, amounts, and distribution of surfaces and natural organic material within a single particle leads to sites with varying affinities for the adsorbing species. Using both model and natural solids, this investigation examines sorption on solids with both homogeneous and heterogeneous surface compositions. While compositional heterogeneity may be a contributing factor to isotherm nonlinearity, structural heterogeneity in the form of microporosity is implicated to play a key role affecting isotherm shape.

To simulate conditions throughout much of the vadose zone, isotherms were measured at 100% relative humidity. At this relative humidity, the solids are coated with an adsorbed layer of water, and because of capillary condensation, the internal pores of aggregates are water-filled. Although adsorption of organic vapors under unsaturated conditions has been found to be highly dependent on the water content, above ~90% relative humidity the total uptake of organic sorbates by soils and sediments has been found to be similar to that in saturated systems (*1–5*).

For sorption onto water-coated solids under unsaturated conditions, four mechanisms are normally considered to contribute to the total contaminant uptake. The term 'sorption' incorporates all four mechanisms and is used when the mechanisms cannot—or need not—be distinguished. In unsaturated systems, sorption incorporates the following: (1) adsorption at the solid/solution interface, (2) adsorption at the water surface/vapor interface, (3) partitioning into natural organic matter, and (4) partitioning into the adsorbed water layer associated with the solids. Evidence from this work and the following kinetic study (*15*) implicates a fifth mechanism—adsorption in micropores—contributing to, and in some instances dominating, sorption.

Isotherms were measured in the desorptive direction for chloroform (CF), trichloroethylene (TCE), and tetrachloroethylene (PCE) vapors. Since remediation of soil and groundwater pollution is predicated on contaminant desorption, an understanding of the mechanisms involved in desorption and those responsible for hysteresis is essential for the design and evaluation of remediation schemes.

Background

Isotherm Shape. An issue which is not well-understood is the relationship between solid properties and isotherm shape. Investigations of organic vapor sorption on wet soils near 100% relative humidity have observed both linear (*1, 2, 6*) and nonlinear (*3, 7, 8*) isotherms. One intent of this study was to investigate the mechanisms affecting isotherm shape.

(*A*) *Linear Isotherms.* The simplest isotherm model for saturated systems is the linear sorption model which relates the sorbed-phase concentration, q, to the aqueous concentration, C_w, by

$$q = K_d C_w \tag{1}$$

where K_d is the distribution coefficient and incorporates both adsorption at the mineral surface and partitioning into any natural organic matter. Linear isotherms are often indicative of partitioning into organic matter (*9–12*), but for adsorption onto mineral surfaces, linear isotherms are indicative of surface homogeneity with an abundance of sites having an equal affinity for the adsorbing species.

When sorption takes place from the vapor phase, a vapor sorption analog to K_d can be derived. The linear sorbed/vapor distribution parameter, K_{sv}, can be defined similarly to K_d as

$$q = K_{sv} C_v \tag{2}$$

K_{sv} incorporates all sorption mechanisms, including par-

* Present address: Failure Analysis Associates, 149 Commonwealth Dr., Menlo Park, CA 94025.

0013-936X/94/0928-0053$04.50/0

titioning into the surface-bound water and adsorption at the water/vapor interface—neither of which are incorporated by K_d. The important criterion for significant adsorption at the water/vapor interface is the ratio of the interfacial area to water volume (*16–20*). Because the internal pores of the solids in this study were water-filled, the water/vapor interfacial area was greatly reduced and was approximately equal to the external surface area. Since the external surface areas of the particles in this study were several orders of magnitude below the water/vapor interfacial areas in studies showing significant interfacial adsorption (*16–20*), this mechanism contributes only slightly to the observed uptake here and will be henceforth ignored.

To compare adsorption from solution to partitioning from the vapor phase, K_{sv} can be converted into an equivalent K_d by subtracting the sorbate partitioned into the surface-bound water. If partitioning into the water layer obeys Henry's law and adsorption at the water/vapor interface is ignored, the relation between K_d and K_{sv} is

$$K_d = K_{sv}H_c - W \tag{3}$$

where W is the water loading on the solid, i.e., the volume of water adsorbed per mass of dry solid.

Natural Organic Matter Partitioning. Organic contaminants in the soil may adsorb onto mineral surfaces or partition into natural organic matter. In many instances, the sorption of nonpolar compounds correlates with the organic matter content of the soil (*9*, *13*, *14*). The relationship between K_d and the organic content of the soil, f_{oc}, defines the organic matter partitioning coefficient, K_{oc}, as (*9*)

$$K_d = K_{oc}f_{oc} \tag{4}$$

Organic matter partitioning theory does not always explain the uptake of hydrophobic hydrocarbons when the f_{oc} is very low. The critical f_{oc} below which mineral adsorption dominates over organic matter partitioning, $^*f_{oc}$, has been postulated to depend on both the mineral-specific surface area, S, and the K_{ow} of the sorbate. Based on regressions using silica gel and organic matter as sorbents, McCarty et al. (*21*) have proposed that $^*f_{oc}$ can be approximated by

$$^*f_{oc} = \frac{S}{200(K_{ow})^{0.84}} \tag{5}$$

(*B*) *Nonlinear Isotherms. Langmuir Model.* Although the Langmuir model was formulated to describe monolayer gas adsorption on homogeneous surfaces, its use has been extended to include adsorption from solution (*22*). The equation was developed based on the concept of a constant adsorption energy, characterized by the b coefficient, and a maximum sorption capacity, q_o. The Langmuir model is characterized by linear adsorption at low surface coverages, but becomes nonlinear as adsorption sites approach saturation. The Langmuir equation takes the form (*23*)

$$q = \frac{q_0 b C_w}{(1 + bC_w)} \tag{6}$$

Freundlich Model. The Freundlich model was developed to describe monolayer gas adsorption on heterogeneous solids and is predicated on a distribution of adsorption energies resulting from surface heterogeneities. Although the Freundlich model is considered empirical for adsorption from solution (*22*), it has theoretical implications which provide a basis for understanding nonlinear adsorption. Where there is a distribution of site energies, adsorption preferentially occurs in the highest energy sites, and as surface coverages are increased, successively lower energy sites become occupied. This decrease in the marginal adsorption energy with increasing surface concentration leads to nonlinear isotherms. The Freundlich equation can be expressed as (*24*)

$$q = K_F C_w^{1/n} \tag{7}$$

where K_F is related to the sorption capacity, and the exponent, $1/n$, characterizes the energy distribution of the adsorption sites. A $1/n = 1$ indicates linear adsorption and, therefore, equal adsorption energies for all sites. A $1/n < 1$ indicates a nonlinear isotherm where the marginal adsorption energy decreases with increasing surface concentration.

Porosity. Because pore size can influence both the amount and the kinetics of adsorption, pores have been classified according to size (*25*). Cylindrical pores with diameters <20 Å or slit-shaped pores of this width are classified as micropores. Pores with diameters between 20 and 500 Å are classified as mesopores, while pores >500 Å are classified as macropores. The dividing diameters are not firm, but each class of pores is associated with a characteristic adsorptive behavior. Capillary condensation is associated with mesoporosity, while solids possessing only macroporosity show little or no capillary effects (*26*). Because micropores are of molecular dimensions, several additional factors govern sorption in these pores.

Molecules adsorbed in micropores are subject to stronger field strengths than those adsorbed on flat surfaces (*27*). Adsorption energies are substantially increased due to the superposition of interaction potentials of opposing walls. Based on the Lennard–Jones potential model, Everett and Powl (*28*) calculated adsorption energies as a function of pore diameter and found that for cylindrical pores 5 adsorbate diameters or less in size, adsorption energies increased with decreasing pore size. Pores 3 adsorbate diameters or less possessed significantly increased interaction potentials, and as pore size approaches that of the adsorbate, interaction potentials were calculated to become more than five times those on a flat surface.

The molecular diameters of the three adsorbates used in this study are ~7 Å (based on the molar volume at the normal boiling point as in ref *29*). Therefore, pores with diameters ~20 Å or less are expected to have increased adsorption energies and, therefore, show increased sorption. According to Freundlich isotherm theory, this distribution of adsorption energies as pores approach molecular dimensions should lead to nonlinear isotherms with $1/n < 1$.

Experimental Section

Adsorbent and Adsorbate Characterization. To assess the effects of contaminant and solid properties on sorption behavior, the solids and the sorbates in this study were chosen to span a range in physical properties. Six model solids, two aquifer solids, and one soil were used to investigate the mechanisms governing sorption of nonpolar organic sorbates on soils and sediments. The solids were characterized with respect to natural organic matter content, surface area, intraaggregate pore size distribution, and particle size. The f_{oc} of each solid was measured by combustion by Desert Analytics (Tucson, AZ). Surface areas were measured by the BET method (*30*), using

Table 1. Physical Properties of the Adsorbents Used

solid	surface area[a] (m^2/g)	EGME S.A. (m^2/g)	organic content[b] (%)	water loading (mL/g)	internal porosity (mL/g)	pore diameter[c] (Å)	particle diameter[d] (μm)
montmorillonite	29	702	0.071	0.30	*e*	*e*	<75[e]
glass beads	0.06	*g*	0	0.074	*g*	*g*	210
silica gel A	297	500	0	0.89	0.76	60	330[f]
silica gel B	268	428	0	1.12	1.10	150	330[f]
silica gel C	394	702	0	0.82	0.76	60	97[f]
silica gel D	242	430	0	1.59	1.70	300	97[f]
Livermore sand	13	67	0.064	0.44	0.54	69	150
Livermore clay & silt	29	141	0.11	0.13	*e*	*e*	<75[e]
Santa Clara	12	67	0.15	0.041	0.060	65	240
Norwood	55	516	1.40	0.15	0.145	65	220

[a] BET method using nitrogen adsorption. [b] Zero indicates below detection limit of 0.001%. [c] Median diameter based on surface area using measured pore size distribution. [d] Sauter mean diameter (*42*) based on ASTM method (*43*). [e] Measured properties not representative of moist solids due to swelling clays. [f] Monodisperse size distribution, i.e., within a single screen size. [g] Properties not within limits of analytical methods.

nitrogen as the adsorbate, and by EGME adsorption (*31*). Intraaggregate porosity was measured by mercury intrusion for pore diameters >30 Å, and by nitrogen desorption for pores between 20 and 30 Å. Due to limitations of the analytical methods, pores less than 20 Å in diameter could not be measured directly, but could be inferred from measurements of nitrogen adsorption.

The clay mineral montmorillonite was chosen as a model solid for its high energy surface and homogeneous composition and lack of internal porosity. Although montmorillonite is an expanding clay mineral, it is effectively nonporous for adsorption of nonpolar organic compounds because adsorbate polarity is required for penetration between clay layers (*32*). The montmorillonite was obtained from the Clay Mineral Society Source Clays Repository (Department of Geology, University of Missouri, Columbia) as samples of SWy-1.

Four porous silica gels (Davisil, Alltech) of the same material were used to examine the effect of pore size and particle size on sorption. The silica gels were measured to be mesoporous with pore size distributions ranging from 20 to 300 Å. Although microporosity on the silica gels could not be measured directly, all types of amorphous silica produced in an aqueous medium possess some degree of microporosity (*27*). Additionally, measurements of nitrogen adsorption revealed high BET energy parameters indicative of microporosity (*33*).

To investigate sorption on a microporous solid lacking meso- and macroporosity, borosilicate glass beads (Alltech) were used. Nitrogen adsorption on the glass beads indicated no mesoporosity. Microporosity could not be directly measured, but nitrogen adsorption measurements provided two strong indications of glass bead microporosity. According to Gregg and Singh (*33*), BET energy parameters greater than 200 and excessively large BET surface areas for nitrogen adsorption are both strong indicators of sorbent microporosity. The nitrogen BET energy parameter for the glass beads was 273 (average of duplicates), and the BET surface area was ~6 times greater than that expected based on the measured particle size and spherical geometry.

The aquifer solids were obtained from contaminated aquifers in the Santa Clara and Livermore Valleys of north central California. The Santa Clara solids were previously characterized by Grathwohl (*34*) and consisted of fragments of sedimentary rocks (54%), single mineral grains (30%), and igneous and metamorphic rock fragments (16%) comprising the remainder. The Livermore Aquifer solids can be characterized as low natural organic matter sediment consisting of sand-sized aggregates in a matrix of clay and silt.

Table 2. Physical and Chemical Properties of CF, TCE, and PCE

property	CF	TCE	PCE	ref
molecular weight (g/mol)	119.38	131.39	165.85	
aqueous solubility at 20 °C (mol/L)	0.071	0.0083	0.00091	44
vapor pressure at 30 °C (kPa)	32.8	12.5	4.28	45
Henry's constant at 30 °C (–)	0.187	0.495	0.924	46
log (K_{ow}) at 23 °C (–)	1.90	2.42	2.53	47
av molecular diameter (Å)	6.4	6.8	7.2	29

Isotherms were measured on three size fractions of the Livermore solids. The bulk fraction (particle diameter <4.75 mm)—which contained the solids in their *in situ* proportions—was separated into a sand size fraction and a clay and silt-size fraction. The fraction of the bulk material passing through the finest screen (0.075 mm) was designated as the clay and silt fraction. The remainder of the Livermore bulk material was designated as the sand fraction.

The physical properties of the solids are given in Table 1, and the relevant properties of the sorbates are noted in Table 2. The sorbates were obtained from Aldrich and used as received with reported purities of the following: CF (99%+), TCE (99%+) and PCE (99.98%).

Desorption Isotherms. Desorption isotherms for CF, TCE, and PCE were measured using a stepwise batch technique on solids contained in unsaturated stainless steel columns (25 cm × 9 mm i.d.). The solids in the columns were in equilibrium with 100% relative humidity to simulate conditions in the vadose zone. The method used to measure the isotherms is analogous to successive dilution methods for measuring desorption isotherms in saturated systems (*35*). The solids in the columns were allowed to adsorb either CF, TCE, or PCE vapors at ~79% P/P_o saturation and allowed to equilibrate for at least 1 week. To assure reproducibility, duplicate isotherms on each solid were measured. In each case, there was close agreement between the two columns, and the isotherms which follow are composites of duplicates. Sufficient equilibration times were assured by the agreement between duplicate columns with different equilibration periods.

After equilibrating with one of the sorbate vapors, the columns were purged while measuring the sorbate mass and concentration in the column effluent with a flame ionization detector (FID) mounted on a Hewlett-Packard 5890 (HP) gas chromatograph (GC). After purging for periods ranging between 2 and 20 min, the columns were shut-in with stainless steel caps and allowed to equilibrate again for periods ranging from 1 week to 3 months. The effluent plateau concentration at the start of a given

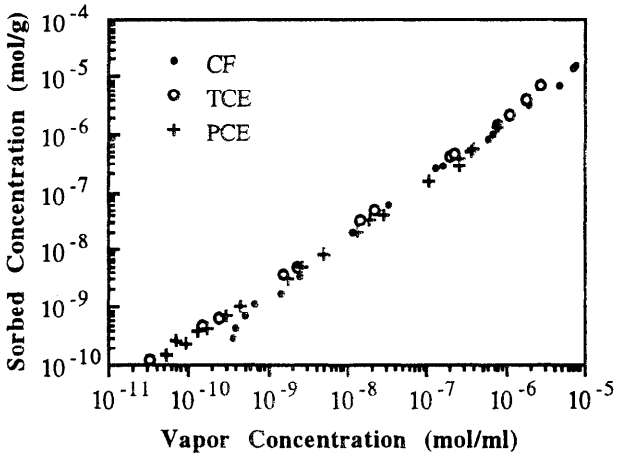

Figure 1. CF, TCE, and PCE vapor sorption on montmorillonite.

purge—as measured by the FID—was equal to the equilibrated sorbate vapor concentration in the column. After ~10 purgings, the sorbate vapor concentration became too low to accurately measure with the FID. At this point, the remaining sorbate was measured by gradually heating the columns (to 180 °C) while purging them with dry nitrogen and trapping the effluent on a column of Tenax (Alltech) adsorbent. The Tenax column was subsequently desorbed by a Tekmar dynamic headspace concentrator and analyzed by an HP 5890 GC equipped with a Hall detector. From the equilibrated vapor concentrations and masses of sorbate removed during each purge, isotherms were generated by summing the masses of sorbate eluted during successive purgings of each column. More detailed descriptions of the methods are contained in refs *36* and *37*.

Results—Model Solids

Nonporous Solids. Figure 1 shows vapor desorption isotherms for CF, TCE, and PCE on montmorillonite. The sorbed concentrations incorporate all modes of uptake and are normalized to the weights of the dry solids. As a function of vapor concentration, the isotherms for all three sorbates coincide and have a slope near unity on the double logarithmic plots. The isotherm slopes on the double logarithmic plots are equivalent to the Freundlich isotherm exponents and are given for all solids in Table 3. The coincidence of the vapor isotherms for all three sorbates is in contrast to the sorption behavior normally observed in saturated systems. Based on the aqueous solubility and K_{ow} of each sorbate, PCE should show the most uptake and CF should show the least. However, because the solids are water-coated, any adsorption onto the mineral surface must occur from solute dissolved in the adsorbed water layer. Therefore, both mineral adsorption and natural organic matter partitioning are dependent on the Henry's constant. For a given vapor concentration, differences in Henry's constants lead to CF having ~5 times higher aqueous concentration than PCE and ~2.5 times higher aqueous concentration than TCE.

Although isotherms based on vapor concentrations coincide for all three sorbates, isotherms based on aqueous partitioning show CF to be the most weakly adsorbed. Figure 2 illustrates this point by showing the amounts sorbed as functions of equivalent aqueous concentrations. The aqueous sorbate concentrations in Figure 2 were calculated from the measured vapor concentrations assuming Henry's law. Although adsorbed water layers may be structured differently than bulk water and therefore deviate from Henry's partitioning, the assumption of Henry's law has been found to be a reasonable approximation on silica gels (*16*) and on soils and sediments (*3*).

(*A*) *Adsorption and Partitioning.* Although it may appear that the high water content of montmorillonite (30% w/w) may allow significant partitioning into the adsorbed water layer, much of the adsorbed water is intercalated between clay layers and is not available for sorbate partitioning. If it is assumed that contaminant partitioning into the adsorbed water obeys Henry's law, the calculated amount of aqueous partitioning exceeds the total sorbate uptake. Therefore, although equivalent aqueous concentrations may be calculated from the measured vapor concentrations, the amount of each sorbate partitioned into the adsorbed water layer cannot be quantitatively assessed.

By assuming that all the sorbate uptake is adsorbed on the solid surface, an upper limit on the fraction of the montmorillonite surface covered with adsorbate can be estimated. For CF which occupies 32.4 Å^2 per adsorbed molecule (*33*), this assumption at the highest vapor concentration leads to 9% coverage of the montmorillonite surface with adsorbed CF. This estimate was based on the nitrogen-measured surface area for dry montmorillonite, which is less than the actual surface area of the moist clays after swelling.

Linear isotherms are often an indicator of organic matter partitioning (*9–12*), and there is a slight amount of natural organic matter (f_{oc} = 0.07%) on the montmorillonite. To assess the contribution of organic matter partitioning, the K_{oc} for each sorbate can be compared to those from other investigations. For example, the log(K_{oc}) values for PCE from 13 studies (summarized by Ball and Roberts in ref *38*) range from 1.8 to 3.1. For PCE sorption on montmorillonite, the log(K_{oc}) value calculated if all the uptake were organic matter partitioning is 3.4. Since this value is higher than the range predicted by the correlations and because the estimated *f_{oc} (0.11%) for PCE is greater than the measured f_{oc} (0.071%), organic matter partitioning likely accounts for only a fraction of the uptake.

This conclusion is supported by several studies showing that for high clay to natural organic matter ratios, mineral adsorption dominates organic matter partitioning (*10, 14*). The ratio of clay to organic matter for adsorption dominance has been found to be related to the hydrophobicity of the solute (*10*). For a log(K_{ow}) of 2.14, the critical clay to organic matter ratio is 15:1, but for this montmorillonite the clay to organic matter ratio is greater than 1000:1.

The Freundlich parameters in Table 3 for the isotherms in Figure 1 show that partitioning on the montmorillonite is linear ($1/n \sim 1$). The montmorillonite is composed of a single mineral type, and the data are consistent with Freundlich isotherm theory in that homogeneous surfaces lead to linear isotherms. Because at low surface coverages the Langmuir model predicts linear adsorption, Langmuir isotherm theory is also consistent with the montmorillonite isotherms. Since the montmorillonite surface area is external and the solids lack any microporosity, there should be no enhanced adsorption and isotherm nonlinearity resulting from microporosity. Thus, for montmorillonite, the data are consistent with all three theories explaining isotherm linearity. However, data from the remaining solids are not consistent with either the Langmuir or

Table 3. Freundlich Model Parameters and Correlation Coefficients Based on Vapor Partitioning for All Solids

	CF			TCE			PCE		
solid	$1/n$	K_F	r^2	$1/n$	K_F	r^2	$1/N$	K_F	r^2
Montmorillonite	1.04	2.37	0.998	0.97	1.58	0.999	0.92	0.67	0.997
silica A	0.75	0.95	0.994	0.69	0.35	0.993	0.66	0.11	0.988
Livermore bulk	0.70	0.018	0.985	0.79	0.055	0.955	0.62	0.0048	0.962
Santa Clara	0.41	0.0025	0.941	0.38	0.0027	0.947	0.43	0.0054	0.954
Norwood	0.84	0.46	0.997	0.81	0.42	0.994	0.83	0.55	0.994
Livermore sand				0.65	0.0065	0.989			
Livermore clay				1.01	1.39	0.999			
silica B				0.74	0.51	0.998			
silica C				0.62	0.21	0.996			
silica D				0.76	0.72	0.999			
glass beads				0.93	0.13	0.974			

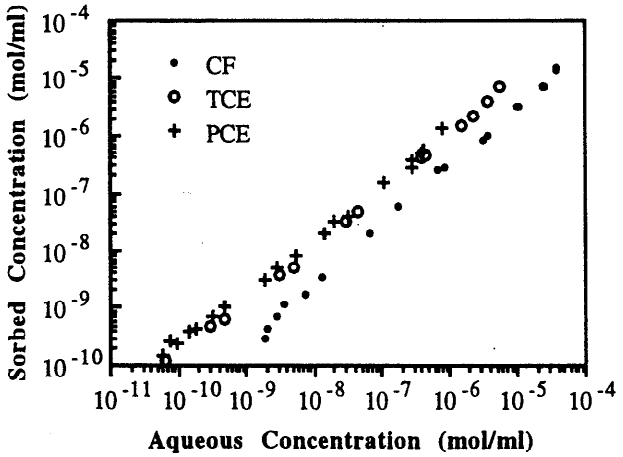

Figure 2. CF, TCE, and PCE sorption on montmorillonite based on aqueous concentrations.

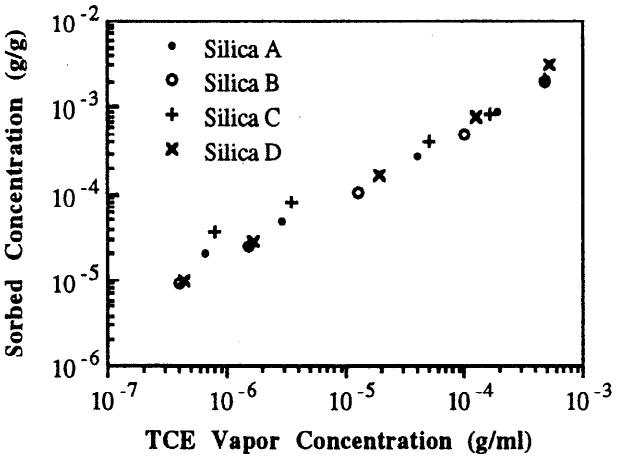

Figure 3. TCE sorption on four silica gels of varying pore and particle size.

Freundlich theories, but are supportive of microporosity-induced nonlinearity.

Meso- and Microporous Solids. Four silica gels of different pore size and particle size were used to investigate the effect of surface area and pore size on adsorption. Like montmorillonite, the silica gels possess a homogeneous surface composition, but unlike montmorillonite, they are porous and contain no organic matter. Figure 3 shows TCE desorption isotherms on four silica gels whose physical properties are summarized in Table 4. Since these silica gels are made of the same material, isotherm differences can only be attributed to pore size, particle size, and surface area differences.

(*A*) *Pore Size and Surface Area.* In Figure 3, the amounts of TCE sorbed at the highest vapor concentrations are independent of the pore size and surface area. At the highest TCE vapor concentration, silicas A, B, and C have identical amounts sorbed, however, silica D shows a higher TCE uptake. Increased sorption on silica D likely results from capillary condensation of TCE in intraparticle pores. The water loading on silica D of 1.59 mL/g was insufficient to completely fill the internal pores, which had a capacity of 1.70 mL/g. The partially water-filled pores had a radius of curvature small enough to allow TCE condensation at 79% P/P_o vapor saturation.

All TCE isotherms on the silica gels were nonlinear with $1/n < 1$ indicating stronger adsorption at lower concentrations. The surface areas of the silica gels inversely correlate with the Freundlich isotherm exponents, but not with the amounts sorbed at the highest TCE concentrations. However, the amounts of TCE sorbed at vapor concentrations below 10^{-5} g/mL do correlate with the surface areas of the silicas. This indicates that the relative contributions of the different sorption mechanisms are functions of the sorbate concentrations.

(*B*) *Adsorption and Partitioning.* The isotherms shown in Figure 3 include both surface adsorption and partitioning into the silica-bound water. Because these silica gels have high water loadings, a significant fraction of the TCE uptake may be partitioned into the sorbed water. If partitioning from the vapor into the adsorbed water layer obeys Henry's law, the amount of sorbate dissolved in the water can be subtracted from the total uptake to generate an isotherm that represents solid surface adsorption only.

Figure 4 shows the TCE isotherm for silica A separated into adsorption at the solid surface and partitioning into the bound water. Because of the overall isotherm nonlinearity, the contribution of aqueous partitioning is greater at higher vapor concentrations and decreases at lower concentrations. At the highest concentration, the assumption of Henry's law leads to 46% of the sorbed TCE partitioned into the aqueous phase and 54% adsorbed on the silica surface. At the lowest concentration, only 6% of the sorbed TCE is in the aqueous phase, while 94% is adsorbed on the solid. Table 4 compares Freundlich exponents for vapor and aqueous partitioning and shows that isotherms based on uptake from aqueous solution have lower exponents than isotherms based on vapor sorption.

From the amount of TCE adsorbed and the area an adsorbed TCE molecule occupies, the fraction of the silica surface covered by TCE can be calculated. Using a value of 43.1 A^2 per molecule of adsorbed TCE (*33*), the fractional surface coverage is less than 1.5% at the highest TCE concentration in Figures 3 and 4.

Although the silica gels are composed of a homogeneous material, silica gel surfaces are composed of two types of

Table 4. Pore Diameter, Surface Area, and Freundlich Isotherm Parameters for Vapor and Aqueous Partitioning on Four Silica Gels

silica	pore diameter (Å)	surface area (m^2/g)	$1/n$ (vapor)[a] (±SE)[c]	K_F (vapor)[a] $(mL/g)^{1/n}$	$1/n$ (aqueous)[b] (±SE)[c]	K_F (aqueous)[b] $(mL/g)^{1/n}$
A	60	297	0.69 ± 0.023	0.35	0.61 ± 0.019	0.071
B	150	268	0.74 ± 0.017	0.51	0.64 ± 0.011	0.067
C	60	394	0.62 ± 0.022	0.21	0.55 ± 0.015	0.053
D	300	242	0.76 ± 0.024	0.72	0.71 ± 0.029	0.16

[a] Isotherms based on vapor concentrations. [b] Isotherms based on corresponding aqueous concentrations. [c] SE = ± standard error of linear regressions.

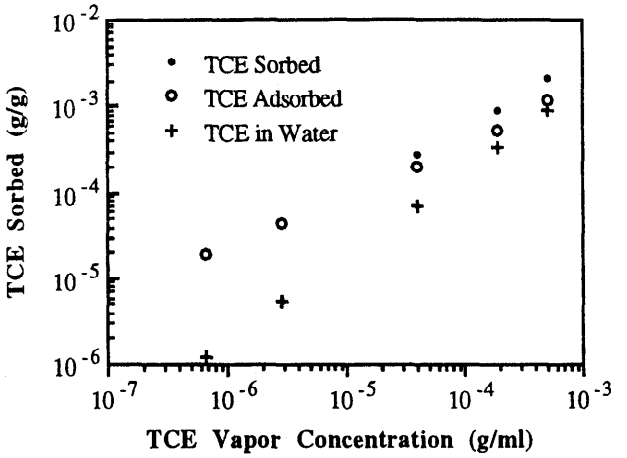

Figure 4. TCE sorbed, adsorbed, and partitioned into bound water on silica A.

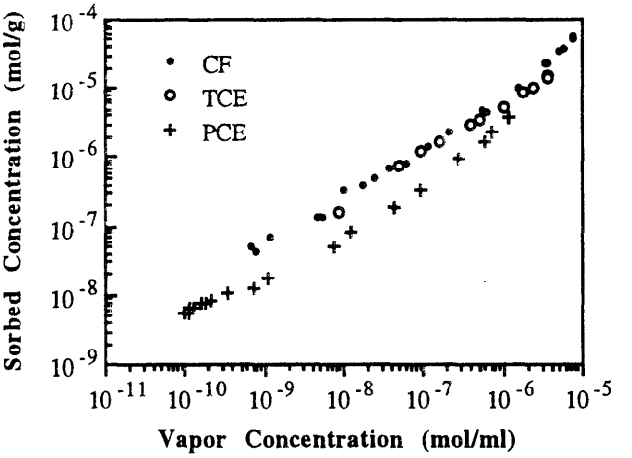

Figure 5. CF, TCE, and PCE vapor sorption on silica A.

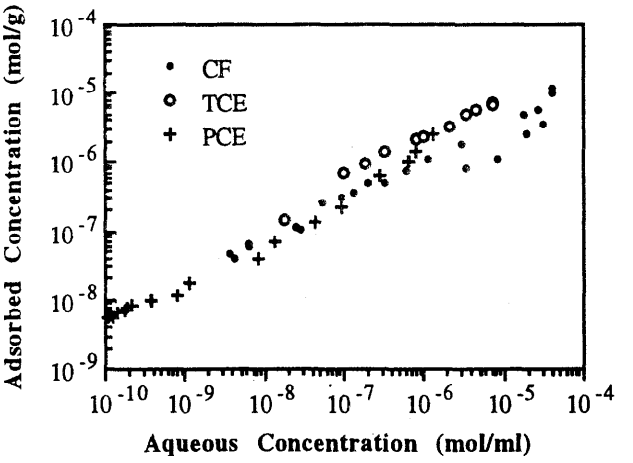

Figure 6. CF, TCE, and PCE adsorbed on silica A based on aqueous concentrations.

sites, high-energy, polar Si-OH (silanol) groups and low-energy, less polar Si-O-Si (siloxane) groups (*33*). Although TCE is relatively less polar than water, it will adsorb more strongly at the polar silanol sites. Preferential adsorption at the polar silanol sites presumably results from the additional dipole–dipole and dipole-induced–dipole attractive forces which are absent at the nonpolar siloxane sites (*39*). The density of these high-energy silanol groups on silica gel has been estimated to be 4.8 groups/100 $Å^2$ (*33*). At the highest TCE concentrations in Figure 3, the TCE coverage is only 0.035 TCE molecules/100 $Å^2$. This indicates saturation of the high-energy sites as concentrations increase cannot account for the silica isotherm nonlinearity.

Because of the low adsorption site coverage, the Langmuir isotherm theory would predict linear adsorption on the silica. Based on an abundance of sites with a uniform energy, the Freundlich model would also predict linear adsorption. Therefore, in contrast to the montmorillonite isotherms, neither the Langmuir nor the Freundlich models are consistent with the nonlinear silica isotherms. However, because these silicas are known to be microporous (*27*), enhanced adsorption due to microporosity is consistent with the nonlinear isotherms.

(*C*) *Silica A Isotherms.* Vapor sorption isotherms for CF, TCE, and PCE on silica gel A are compared in Figure 5. At any vapor concentration, PCE sorbs the least while CF and TCE sorption is nearly the same. The lower uptake for PCE can be attributed to its lower Henry's constant. At any vapor concentration, PCE has a lower aqueous concentration than either CF or TCE. This leads to less PCE partitioned into the silica-bound water and less PCE adsorbed on the surface as compared to CF and TCE.

Assuming Henry's law applies to partitioning into the water, Figure 6 shows the amount of each sorbate adsorbed on the surface as a function of its aqueous concentration. In Figure 6, CF and PCE adsorption is nearly identical while TCE adsorption is marginally greater. Since adsorption on the silica presumably occurs at the polar silanol sites, all three adsorbates are attracted by both dispersion forces and dipole-induced–dipole forces. Since PCE is more hydrophobic than TCE, it might be expected to show higher sorption; however, the permanent dipole of TCE contributes to an additional dipole–dipole attractive force between TCE and the silanol sites. This may explain the greater adsorption of TCE as compared to PCE on the silica.

Microporous Solids. Figure 7 shows isotherms for sorbed and adsorbed TCE on the microporous glass beads. Assuming Henry's law for the aqueous partitioning, the TCE adsorbed on the glass bead surface represents only 12% of the total TCE uptake at the highest concentration. At this TCE concentration, the fractional TCE surface coverage is 24%. This estimate is based on the BET measured surface area which is ~6 times larger than the surface area estimated from the particle size assuming a spherical geometry. Since the actual glass bead surface

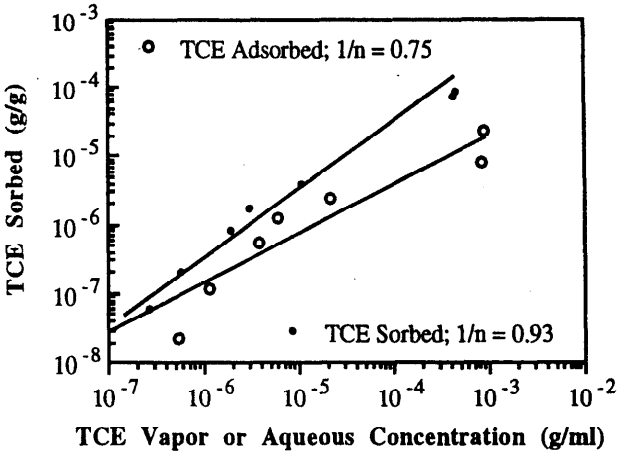

Figure 7. TCE sorbed as a function of vapor concentration, and TCE adsorbed as a function of aqueous concentration on glass beads.

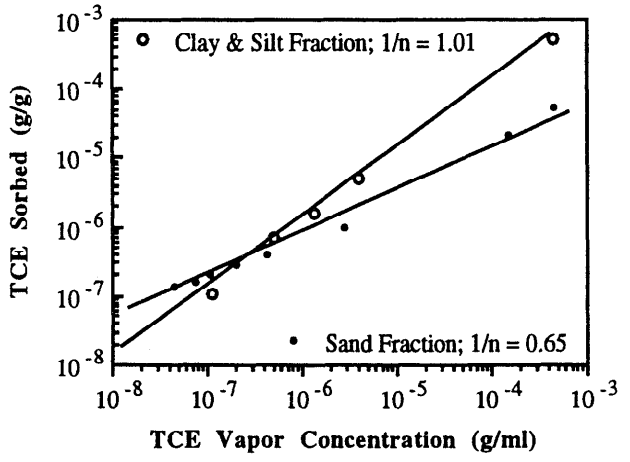

Figure 8. TCE vapor sorption isotherms with Freundlich isotherm exponents for the clay and silt and the sand fractions of the Livermore solids.

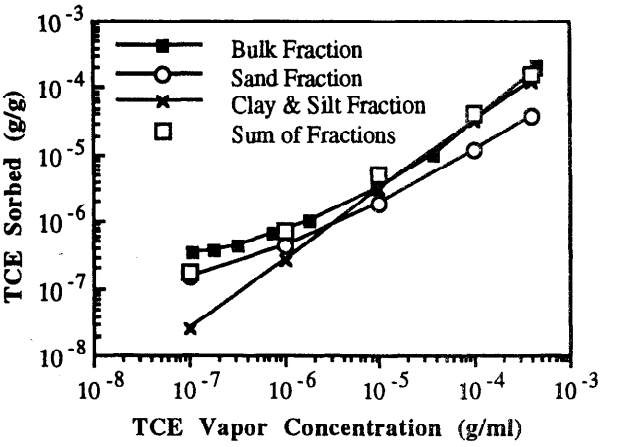

Figure 9. TCE vapor isotherms on the bulk, sand, and clay and silt fractions of the Livermore solids compared with the composite *sum of the fractions* isotherm.

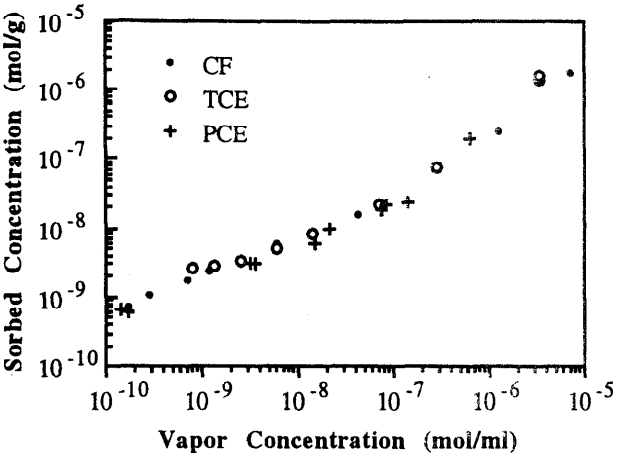

Figure 10. CF, TCE, and PCE vapor sorption on the bulk fraction of the Livermore aquifer solids.

area is likely to be less than the BET measured area, the fractional TCE surface coverage may be much greater than the estimated 24%. However, even a 24% surface coverage is 16 times greater than that on the silica gels and indicates that, on microporous solids, adsorption may be greater than estimated based on the measured surface area.

Results—Natural Materials

Livermore Aquifer Solids. (*A*) *Size Fractions.* To assess how the individual size fractions contribute to the sorption behavior of the bulk material, TCE isotherms were measured separately on the bulk fraction, the sand fraction, and the clay and silt fraction of the Livermore Aquifer solids. Vapor isotherms for the sand and the clay and silt fractions are shown in Figure 8 along with their fits to the Freundlich equation. The clay and silt isotherm has a Freundlich exponent near 1 indicating linear sorption, but the sand fraction has a $1/n = 0.65$, indicating nonlinear sorption.

Possible factors contributing to the different isotherm shapes of the two size fractions include differences in f_{oc}, mineral composition, and internal porosity. Differences in natural organic matter content are not likely to have significant impact since the f_{oc} of both fractions are close to the $*f_{oc}$ of 0.06% for the sand and 0.13% for the clay and silt. Since homogeneous surfaces do not necessarily lead to linear isotherms, mineralogical homogeneity of the clay and silt fraction cannot completely account for the linear isotherm on that fraction.

Of all the solids studied, only the montmorillonite and the Livermore clay and silt isotherms were linear. Because of their small particle size, both the montmorillonite and the Livermore clay and silt have substantial external surface areas. This coincidence may indicate that the linearity of the Livermore clay and silt isotherm results from adsorption on external surfaces, which is not subject to micropore induced nonlinearity.

Isotherms for the two Livermore size fractions can be combined to generate a composite isotherm for the bulk material. The bulk material is composed of 75% sand fraction and 25% clay and silt fraction. Combining the isotherm for each size fraction in proportion to its contribution to the bulk material yields the *sum of the fractions* isotherm denoted by the open squares in Figure 9. Both composite isotherms are more linear on the logarithmic plot than is their sum, illustrating how isotherm shape can be influenced by heterogeneity of the bulk material. The composite *sum of the fractions* isotherm compares well to the actual bulk isotherm except at the lowest concentration. Above 10^{-5} g/mL TCE vapor concentration, the clay and silt fraction dominates TCE uptake while below 10^{-7} g/mL, the sand fraction dominates.

(*B*) *Bulk Fraction.* Vapor isotherms for CF, TCE, and PCE on the Livermore bulk fraction are compared in Figure 10. All three isotherms are nonlinear as indicated by their Freundlich exponents given in Table 3. The data for all three isotherms overlap and deviate systematically from the Freundlich model in that they decrease in slope

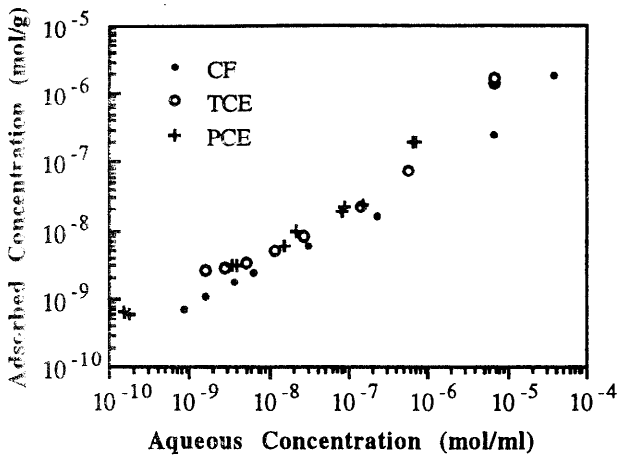

Figure 11. CF, TCE, and PCE adsorption on the bulk fraction of the Livermore aquifer solids based on aqueous concentrations.

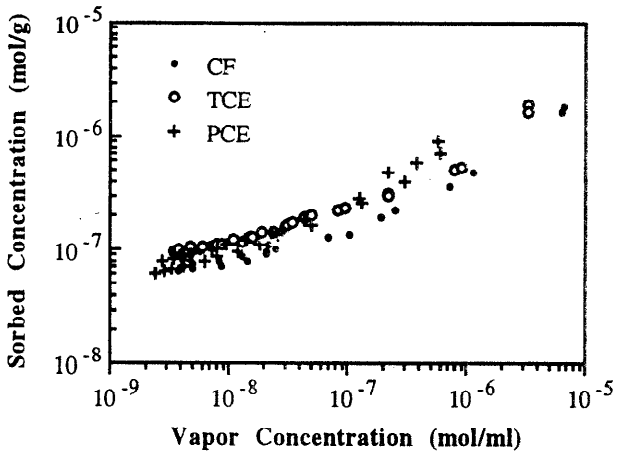

Figure 12. CF, TCE, and PCE vapor sorption on the Santa Clara aquifer solids.

with decreasing concentration on the logarithmic plots. This isotherm curvature might be explained in terms of a distribution of adsorption energies different from the distribution assumed by the Freundlich model. However, in light of the data in Figure 9, deviation from the Freundlich model can be explained by the superposition of isotherms for the different size fractions. As measured by the correlation coefficients given in Table 3, isotherms for solids with monodisperse particle sizes (Figures 1, 3, 5 and 7) more closely followed the Freundlich model than did isotherms for solids with wider particle size distributions.

The low water content of the Livermore bulk solids results in very little sorbate partitioned into the adsorbed water, and thus nearly all the uptake is adsorption on the mineral surface. Assuming that all the uptake is adsorbed on the surface, the fraction of the surface covered by sorbate at the highest concentrations is less than 2%. However, because adsorption on the mineral surface must occur from solute dissolved in the adsorbed water, Henry's constants and aqueous partitioning still influence the sorbate uptake.

Figure 11 compares isotherms for CF, TCE, and PCE adsorbed on the surface of the Livermore bulk solids based on concentrations in the adsorbed water layer. As functions of aqueous concentration, isotherms for the three sorbates no longer coincide, and CF adsorbs less than both TCE and PCE, which adsorb similar amounts.

Santa Clara Solids. Vapor sorption isotherms for CF, TCE, and PCE on the Santa Clara Aquifer solids are shown in Figure 12. Of all the solids in this study, the isotherms for the Santa Clara solids are the most nonlinear as shown by their Freundlich exponents in Table 3. For TCE, the nonlinearity results in the ratio of sorbed to vapor concentration increasing by a factor of ~50 between the first and last points of the isotherm. Unlike on the montmorillonite and Livermore solids, the vapor isotherms for the three sorbates on the Santa Clara solids do not coincide. For all but the lowest vapor concentrations, CF adsorbs less than both TCE and PCE. Below $\sim 10^{-7}$ mol/mL of vapor concentration, the isotherms for the three sorbates flatten and begin to converge. When the isotherms are plotted as functions of aqueous concentration as in Figure 13, CF clearly adsorbs less than both TCE and PCE. The extreme nonlinearity and isotherm flattening indicate the presence of strongly adsorbing sites with a sorption capacity near $\sim 7 \times 10^{-8}$ mol/g.

To investigate whether hysteresis contributes to the nonlinearity, adsorption and desorption isotherms were

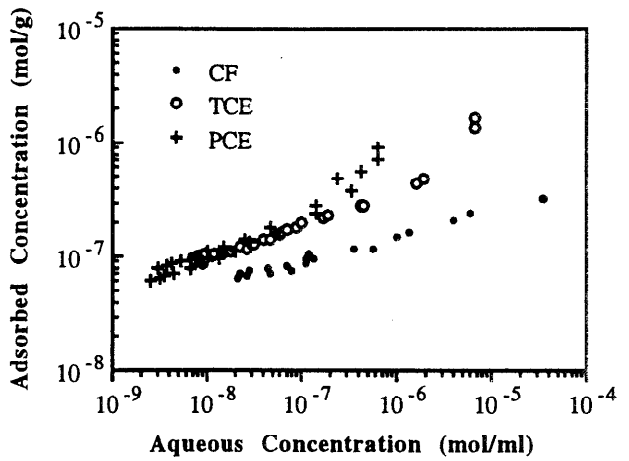

Figure 13. CF, TCE, and PCE adsorption on the Santa Clara aquifer solids based on aqueous concentrations.

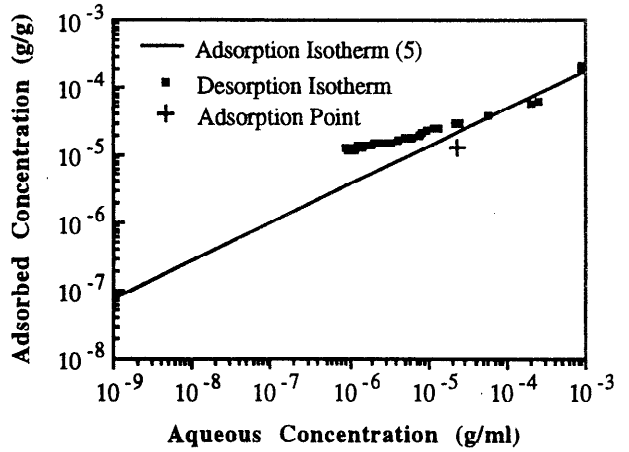

Figure 14. Comparison of adsorption and desorption isotherms for TCE on the Santa Clara solids.

compared for TCE on the Santa Clara solids. Grathwohl and Reinhard (5) measured TCE adsorption from aqueous solution on the Santa Clara solids for aqueous concentrations between 10^{-9} and 10^{-3} g/mL. The adsorption isotherm fit the Freundlich model with an $r^2 > 0.99$ and an isotherm exponent of $1/n = 0.56$. Figure 14 compares the adsorption isotherm of Grathwohl and Reinhard to the desorption isotherm measured in this study. Also shown in Figure 14 is a single data point (denoted by a '+') measured in the adsorptive direction by the methods used in this study. Both the single adsorption data point and the adsorption isotherm indicate the presence of hysteresis.

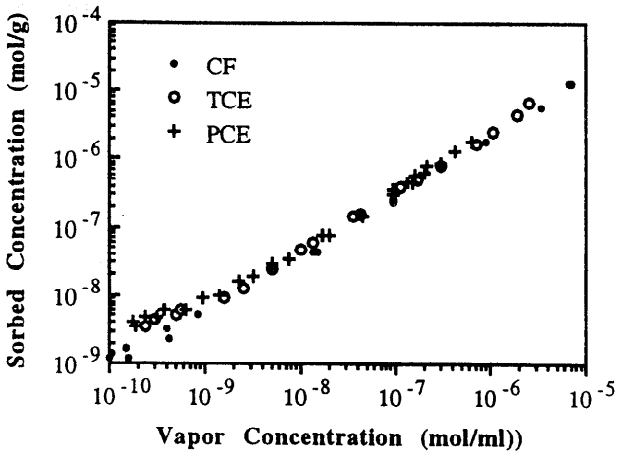

Figure 15. CF, TCE, and PCE vapor sorption on Norwood soil.

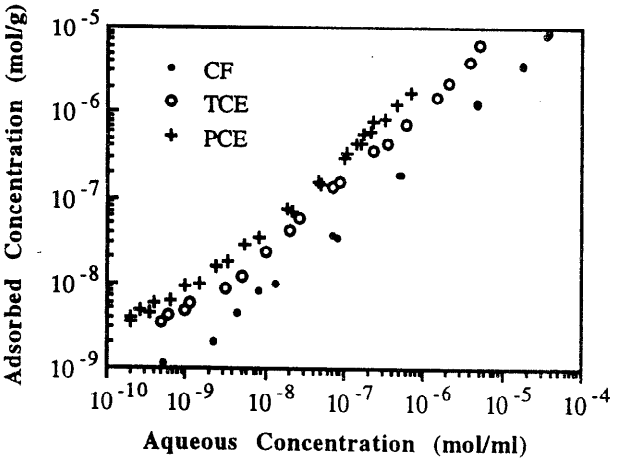

Figure 16. CF, TCE, and PCE adsorption on Norwood soil based on aqueous concentrations.

For the single adsorption data point, the amount of uptake is a factor of ~2 lower on the adsorption branch compared to the desorption branch of the isotherm, and this difference increases with decreasing concentration.

To assure that the hysteresis in Figure 14 was not an experimental artifact of insufficient equilibration times, periods of up to 3 months were allowed between successive purgings of the two columns. Equilibration periods of 1 and 3 months were found to give identical results, and more than 11 months elapsed between the first and last isotherm points in Figure 14.

Aside from experimental artifacts, hysteresis is most often attributed to irreversible sorption in organic matter (*40*). Several studies have found that the extent of hysteresis is in proportion to the f_{oc} of the soil (*40*, *41*). However, for the Santa Clara solids, the very low f_{oc} (0.15%) and the nonlinearity of the adsorption isotherm ($1/n$ = 0.56) both make it less likely that the hysteresis results from organic matter partitioning. If the TCE uptake on the Santa Clara solids were due to irreversible organic matter sorption, greater linearity (i.e., a $1/n$ closer to 1) would be expected for the uptake isotherm. Furthermore, irreversible sorption was not observed and all the sorbed TCE was removed by heating the solids.

Norwood Soil. Figure 15 compares vapor adsorption isotherms for CF, TCE, and PCE on Norwood soil. Like the montmorillonite and Livermore isotherms, the isotherms for all three sorbates coincide on the Norwood soil. Of the three natural solids, the Norwood isotherms are the most linear as indicated by their larger Freundlich exponents given in Table 3. The greater linearity of the Norwood isotherms, compared to the Santa Clara and Livermore bulk isotherms, may indicate that organic matter partitioning dominates sorbate uptake. Equation 5 predicts that the f_{oc} of the Norwood soil is >2 times higher than the $*f_{oc}$ for CF sorption and >7 times higher than the $*f_{oc}$ for PCE. Further evidence for organic matter partitioning on the Norwood soil can be seen when the isotherms are plotted as functions of the corresponding aqueous concentrations as in Figure 16.

Organic matter partitioning theory predicts that for a given aqueous concentration, PCE (K_{ow} = 340) should be the highest sorbing, followed by TCE (K_{ow} = 260), and CF (K_{ow} = 80). This behavior was followed only on the Norwood soil which has at least a 9 times higher f_{oc} than any other solid. When expressed as functions of aqueous concentration, the montmorillonite, Livermore, and Santa Clara solids showed less CF adsorption but little difference between TCE and PCE adsorption. This may indicate that mineral adsorption accounts for the uptake on these solids.

Discussion

Based on vapor concentrations, isotherms for the total uptake of all three sorbates coincided on the montmorillonite, Norwood, and Livermore solids. On all but the Norwood soil—where organic matter partitioning was likely responsible for most of the uptake—mineral adsorption was the dominant sorption mechanism. Linear adsorption isotherms were observed on the nonporous solid (montmorillonite) and on the solids with the highest external surface area (Livermore clay and silt). This may indicate that on water coated minerals, adsorption on external surfaces absent of microporosity is linear. Based on Langmuir and Freundlich isotherm theories: at low adsorption densities mineral adsorption is expected to be linear on homogeneous solids such as the silica gels, glass beads, and montmorillonite. However, on the glass beads and silica gels, adsorption was nonlinear. Since silica gels are known to be microporous (*27*), and microporosity was indicated on the glass beads, structural heterogeneity in the form of micropores is consistent with the nonlinear isotherms. The inverse correlation of the Freundlich isotherm exponents with the surface area of the silicas may indicate that microporosity is distributed over the amorphous silica surfaces.

Cooperative effects between neighboring molecules adsorbed in small pores may contribute to nonlinearity in the desorption isotherms. Because sorption of an organic species in a water-filled pore of molecular dimensions creates a more lipophilic environment, hydrophobicity of the solute may lead to further sorption in that pore. For organic species adsorbed in a lipophilic environment created by their own adsorption in a micropore, desorption is not expected to follow the same path as adsorption. In this case, hysteresis between adsorption and desorption may result from the fact that the nature of the microenvironment has been changed due to the initial adsorption. This hypothesis of cooperative adsorption in micropores is consistent with the observed hysteresis on the Santa Clara Aquifer solids. The highly nonlinear adsorption isotherm ($1/n$ = 0.56) may be indicative of microporosity, and the desorption hysteresis may stem from cooperative effects. However, more work is needed to clarify this issue.

The article which follows (*15*) examines the kinetics of desorption from these solids. The isotherms and ideas

presented here form the basis for interpreting the desorption kinetics data.

Glossary

b	Langmuir intensity coefficient (L^3/M_a)
C_v	vapor concentration of adsorbate (M_a/L^3)
C_w	concentration of adsorbate in solution (M_a/L^3)
f_{oc}	mass fraction of organic carbon (M_{oc}/M_s)
$^*f_{oc}$	critical organic content (M_{oc}/M_s)
H_c	Henry's constant (C_v/C_w) (–)
K_d	solid/solution distribution coefficient ($(M_a/M_s)/(M_a/L^3)$)
K_F	Freundlich capacity coefficient ($\{(M_a/M_s)/(M_a/L^3)\}^{1/n}$)
K_{oc}	organic carbon partitioning coefficient (L^3/M_{oc})
K_{ow}	octanol/water partitioning coefficient (–)
K_{sv}	sorbed/vapor distribution coefficient ($(M_a/M_s)/(M_a/L^3)$)
L	length dimension
M_a	mass of adsorbate
M_{oc}	mass of organic carbon
M_s	mass of solids
$1/n$	Freundlich exponent (–)
P	vapor pressure
P_o	saturation vapor pressure
q	sorbed concentration (M_a/M_s)
q_o	Langmuir capacity coefficient (M_a/M_s)
S	specific surface area of the solid (m^2/g)
W	volume of adsorbed water per weight of dry solid (L^3/M_s)

Acknowledgments

This work was supported in part by the U.S. EPA Office of Exploratory Research, Washington, DC, under Agreement R-815738–01 through the Western Region Hazardous Substance Research Center. Additional support was provided by Lawrence Livermore National Laboratories through B116830. The authors thank Charles Werth for his contribution to characterization of the solids and George M. Deeley of Shell Development Co. for providing us with the Norwood soil. The content of this paper does not necessarily represent the views of the supporting organizations.

Literature Cited

(1) Chiou, C. T.; Shoup, T. D. *Environ. Sci. Technol.* **1985**, *19*, 1196.
(2) Peterson, M. S.; Lion, L. W.; Shoemaker, C. A. *Environ. Sci. Technol.* **1988**, *22*, 571.
(3) Grathwohl, P. Doctoral Dissertation, University of Tubingen, Tubingen, Germany, 1989.
(4) Ong, S. K.; Lion, L. W. *Water Res.* **1991**, *25*, 29.
(5) Grathwohl, P.; Reinhard, M. Environ. *Sci. Technol.* **1993**, *27*, 2360.
(6) Chiou, C. T.; Kile, D. E.; Malcolm, R. L. *Environ. Sci. Technol.* **1988**, *22*, 298.
(7) Call, F. *J. Sci. Food Agric.* **1957**, *8*, 630.
(8) Call, F. *J. Sci. Food Agric.* **1957**, *8*, 137.
(9) Karickhoff, S. W.; Brown, D. S.; Scott, T. A. *Water Res.* **1979**, *13*, 241.
(10) Karickhoff, S. W. *J. Hydraul. Eng.* **1984**, *110*, 707.
(11) Chiou, C. T.; Potter, P. E.; Schmedding, D. W. *Environ. Sci. Technol.* **1983**, *17*, 227.
(12) Chiou, C. T.; Shoup, T. D.; Porter, P. E. *Org. Geochem.* **1985**, *8*, 9.
(13) Chiou, C. T.; Peters, L. J.; Freed, V. H. *Science* **1979**, *206*, 831.
(14) Weber, W. J.; McGinley, P. M.; Katz, L. E. *Environ. Sci. Technol.* **1992**, *26*, 1955.
(15) Farrell, J.; Reinhard, M. *Environ. Sci. Technol.*, following paper in this issue.
(16) Dorris, G. M.; Gray, D. G. *J. Chem. Sci. Faraday Trans.* **1981**, *77*, 725.
(17) Dorris, G. M.; Gray, D. G. *J. Phys. Chem.* **1981**, *85*, 3628.
(18) Katz, S.; Gray, D. G. *J. Colloid Interface Sci.* **1981**, *82*, 326.
(19) Katz, S.; Gray, D. G. *J. Colloid Interface Sci.* **1981**, *82*, 339.
(20) Karger, B. L.; Castells, R. C.; Sewell, P. A.; Hartkopf, A. *J. Phys. Chem.* **1971**, *75*, 3870.
(21) McCarty, P. L.; Reinhard, M.; Rittmann, B. E. *Environ. Sci. Technol.* **1981**, *15*, 40.
(22) Adamson, A. W. *Physical Chemistry of Surfaces*, 4th ed.; John Wiley & Sons: New York, 1984.
(23) Langmuir, I. *J. Am. Chem. Soc.* **1918**, *40*, 1361.
(24) Freundlich, H. *Colloid Capillary Chemistry*; Methuen: London, 1926.
(25) IUPAC. Manual of Symbols and Terminology. *Pure Appl. Chem.* **1972**, *31*, 578.
(26) Dubinin, M. M. In *Characterisation of Porous Solids*; Gregg, S. J., Sing, K. S. W., Eds.; Society of Chemical Industry: London, 1979.
(27) Kiselev, A. V. *Discuss. Faraday Soc.* **1971**, *52*, 14.
(28) Everett, D. H.; Powl, J. C. J. *Chem Soc. Faraday Trans. 1* **1976**, *72*, 619.
(29) Prasher, B. D.; Ma, Y. A. *AIChEJ* **1977**, *23*, 303.
(30) Brunauer, S.; Emmett, P. H.; Teller, E. *J. Am. Chem. Soc.* **1938**, *60*, 309.
(31) Carter, D. L.; Heilman, M. D.; Gonzalez, C. L. *Soil Sci.* **1965**, *100*, 356.
(32) Parfitt, R. L.; Greenland, D. J. *Clay Miner.* **1970**, *8*, 305.
(33) Gregg, S. J.; Singh, K. S. W. *Adsorption, Surface Area, and Porosity*; Academic Press: New York, 1982.
(34) Grathwohl, P. Sorption and Desorption Kinetics of Trichloroethylene in Aquifer Material Under Saturated and Unsaturated Conditions. Western Region Hazardous Substance Research Center, Technical Report No. WRC-2, 1991.
(35) Rao, P. S. C.; Davidson, J. M.; Jessup, R. E.; Selim, H. M. *Soil Sci. Am. J.* **1979**, *43*, 22.
(36) Farrell, J.; M. Reinhard. In *Current Practices in Ground Water and Vadose Zone Investigations*; Nielsen, D., Sara, M., Eds.; ASTM: Philadelphia, 1991.
(37) Farrell, J. Ph.D. Dissertation, Stanford University, 1993.
(38) Ball, W. P.; Roberts, P. V. *Environ. Sci. Technol.* **1991**, *25*, 1223.
(39) Prausnitz, J. M.; Lichtenthaler, R. N.; de Azevedo, E. G. *Molecular Thermodynamics of Fluid Phase Equilibria*, 2nd ed.; Prentice Hall: Englewood Cliffs, NJ, 1986.
(40) Bowman, B. T.; Sans, W. W. *J. Environ. Qual.* **1985**, *14*, 270.
(41) Peck, D. E.; Corwin, D. L.; Farmer, W. J. *J. Environ. Qual.* **1980**, *9*, 101.
(42) Foust, A. S.; et. al. *Principles of Unit Operations*, 2nd ed.; John Wiley & Sons: New York, 1980.
(43) ASTM. *Manual on Test Sieving Methods*; ASTM: Philadelphia, 1985.
(44) Horvath, A. L. *Halogenated Hydrocarbons: Solubility-Miscibility with Water*; Marcel-Dekker: New York, 1982.
(45) Jordan, T. E. *Vapor Pressure of Organic Compounds*; Interscience: New York, 1954.
(46) Gossett, J. M. *Environ. Sci. Technol.* **1987**, *21*, 202.
(47) Banerjee S.; Yalkowsky, S. H.; Valvani, S. C. *Environ. Sci. Technol.* **1980**, *14*, 1227.

Received for review March 11, 1993. Revised manuscript received September 21, 1993. Accepted October 4, 1993.•

• Abstract published in *Advance ACS Abstracts*, November 15, 1993.